Mapping of the Evaporative Loss From Elephant Butte Reservoir Using Remote Sensing and GIS Technology

by
Alex Herting
Tim Farmer
Jordan Evans

December 3, 2004

TABLE OF CONTENTS ════════════

Table of Figures

List of Tables ━━━━━━━━━━━━━━

ACKNOWLEDGEMENT

INTRODUCTION

This report pertains to the mapping of evaporative loss from Elephant Butte Reservoir using remote sensing and GIS technology. Elephant Butte Reservoir is located in south central New Mexico, near the town of Truth or Consequences. Elephant Butte Dam was constructed on the Rio Grande River in 1916 to provide irrigation and flood control. The resulting lake is approximately 4 miles wide and 40 miles long and is enjoyed by millions of New Mexicans each year seeking recreation. This includes fishing, water skiing, swimming, and many other water-sports. There are many bass tournaments held at Elephant Butte each year. Figure 1 shows a picture of Elephant Butte Dam and reservoir.
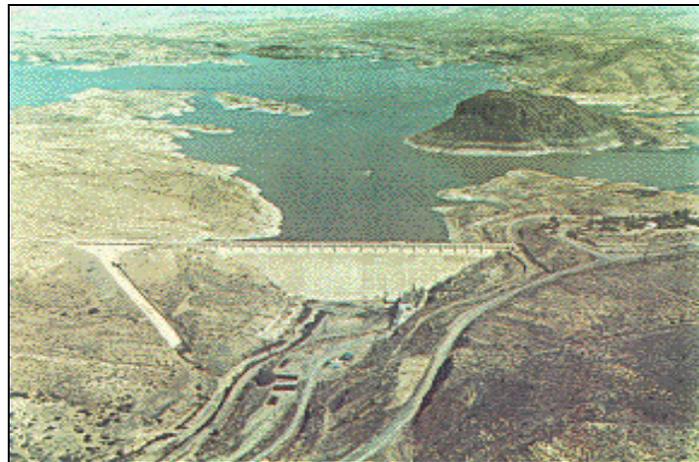
Figure 1. Elephant Butte Dam and Reservoir

The headwaters of the Rio Grande River begin in Colorado and then wind through the Southwest approximately 1800 miles and ends in the Gulf of Mexico. The Rio Grande runs from north to south through the State of New Mexico. This river passes through several dams and reservoirs on its journey, but Elephant Butte is the largest reservoir in the State of New Mexico. Figure 2 shows a picture of the Rio Grande river.

Figure 2. Rio Grande River

The capacity of Elephant Butte reservoir is estimated to be over two million acre-feet. The inflow to the lake ranges from approximately 114,100 to 2,831,000 acre-feet per year. The average inflow to this reservoir is approximately 900,000 acre-feet per year. Evaporation from the lake is estimated to be as much as 1/3 of the approximate average inflow, which would be approximately 250,000 acre-feet per year. See Figure 3 for a graph of average annual evaporation values.

Figure 3. Annual Evaporation Data

The situation at Elephant Butte Reservoir is similar to the largest lake in Egypt, but at a much smaller scale. The Nasser Lake in Upper Egypt loses approximately 10 million acre-feet per year due to evaporation (Shaltout and Housry, 1996). At any scale, evaporation is a quantitatively major loss term, so to monitor this loss; the Bureau of Reclamation (BOR) currently uses a Class A Evaporation pan to estimate the evaporation from Elephant Butte. Pan evaporation is notoriously unreliable due to the metal pan, wh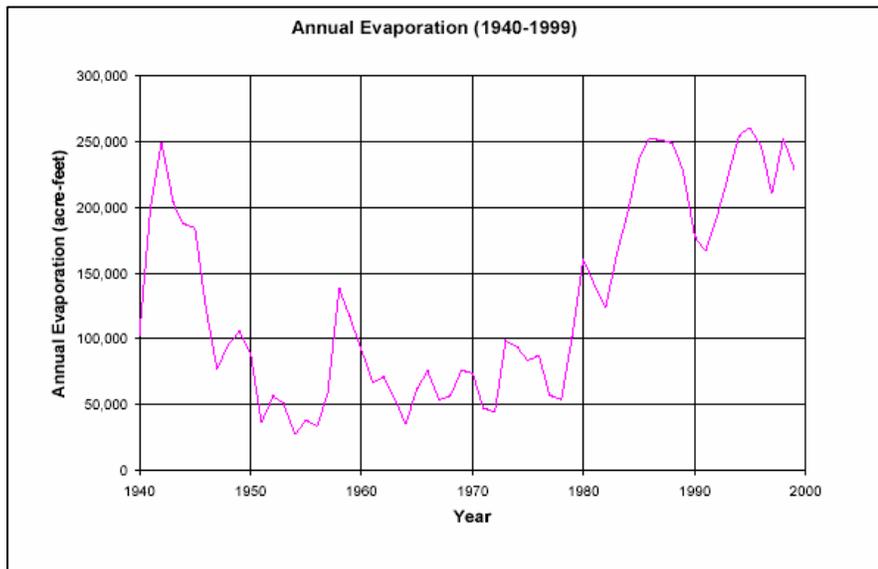ich can heat up and lead to large errors in evaporation estimation. Estimation through the use of remote sensing, on the other hand, has the possibility of being very accurate. Better methods for estimating evaporation would lead to better planning and allocation of water. In this region, this would ease tensions between neighboring states and between the United States and Mexico.

EVAPORATION

Quantifying evaporation to a body of water can be very difficult. Depending on the accuracy of measurements sought, the methods used to derive evaporation can become increasingly complex. These methods may be simplified if less accurate results are acceptable. Common equations describing evaporation are the Penman, Hargreave's, and Hamon's equations. Another method, the Bulk-Aerodynamic Method or the mass transfer method, utilizes the skin temperature of water, relative humidity, wind speed, and air temperature to estimate evaporation. This method is fairly accurate, and is the main method utilized in this report. These equations are fully described in the Appendix. Another method for estimating evaporation was created by Shaltout and Housry (1996) for Lake Nasser in Egypt. They discovered that satellite images of Lake Nasser produced accurate temperatures across the skin surface in degrees Kelvin$*10^4$. This method was taken into consideration, since Lake Nasser and Elephant Butte Reservoir have many of the same characteristics. The last method described is pan evaporation, which is currently being used at Elephant Butte Reservoir.

Evaporation is a function of temperature, wind speed, humidity, and radiation. Penman's equation is more detailed than the Hargreave and Hamon equations, and includes all of the listed factors. Hargreave's equation is based on temperature and

radiation of the sun. Hamon's equation is based on temperature and number of sunshine hours. There are also less common equations such as the Papadakis equation that depends on the minimum and maximum saturated air pressures above the surface of the water. Other equations that include some of the same factors as the Papadakis, Hamon, and Hargreave equations are the DeBruin-Keijman, Priestly-Taylor, and the Energy Budget equations. A study done by the University of Georgia compared some of these empirical evaporation equations to one another and to evaporation data from Seminole Lake (Mosner and Aulenbach, 2003). The results are well grouped and show a variation of 2-3 centimeters between equations as seen in Figure 4.
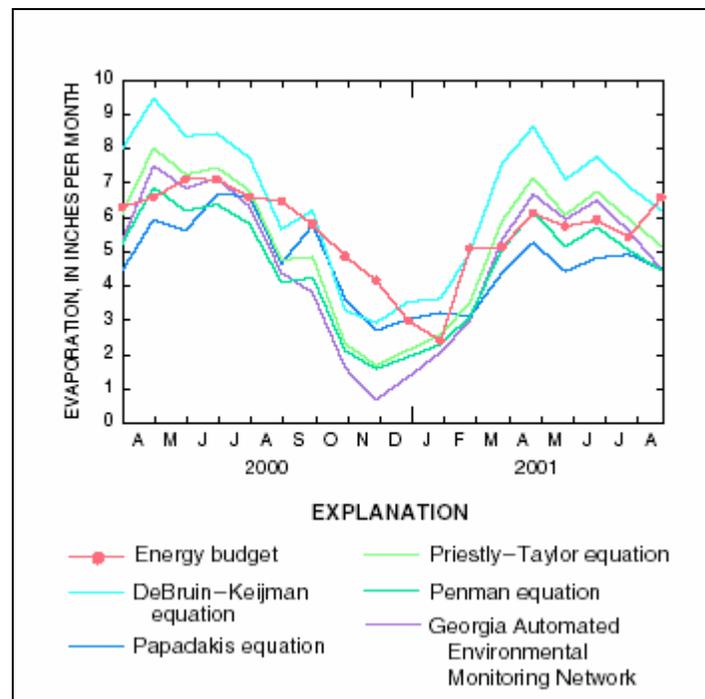
Figure 4. Comparison of Evaporation Equations

The Bulk-Aerodynamic method is also a lesser used method. This method estimates evaporation reasonably accurately, but is dependent on the measurements of the skin temperature of water. The main technique for measuring the skin temperature of water is through an infrared thermocouple on the Elephant Butte Reservoir. With satellite imagery, this method could be greatly enhanced by finding the skin temperature across the entire lake.

Priestly (1982) and his research group from the Federation of Meteorology in Australia have stated that to measure lake evaporation it would "require measurement of

water temperature, wind run, and the temperature/humidity profile immediately above the lake surface." This statement corresponds to the variables in the previously stated equations.

PAN EVAPORATION

Pan evaporation consists of a pan placed near the reservoir, as shown in Figure 5. Readings are taken from the pan as the water level goes down. A coefficient to account for the pan heating up is then multiplied to the reading to give a corresponding amount of reservoir evaporation in inches or millimeters per day. For some days of June, 2003,

Table 1 shows both pan and lake evaporation data. The coefficient currently being used by the BOR is 0.7. This coefficient is used for the whole surface of the lake to give total volumes of water lost to evaporation, which is also shown in Table 1.

Figure 5. Class A Evaporation Pan at Elephant Butte Reservoir

Table 1. June 2003 Evaporation Data for Elephant Butte Reservoir

Day	Pan Evap (Inches)	Net Evap. (Inches)	Elev. (Ft)	Area (Acres)	Evaporation (Acre-Feet)
1	0.59	0.41	4325.84	10501	361
2	0.60	0.42	4325.66	10472	367
3	0.65	0.46	4325.48	10443	396
4	0.55	0.39	4325.32	10417	334
5	0.57	0.4	4325.14	10388	345
27	0.57	0.4	4319.56	9469	315
28	0.50	0.35	4319.34	9423	275
29	0.50	0.35	4319.10	9371	273
30	0.52	0.36	4318.84	9316	283
Total	18.5	12.95			10741
Avg	0.62	0.43			358

There are some major assumptions that must be considered when using this method to estimate evaporation. An assumption is made that evaporation is uniform over the entire surface area of the lake and that the evaporation rate is also uniform throughout the year. These assumptions however are not representative of actual conditions. Linacre (1994) states in a report on evaporation, that the factor (coefficient) is not constant, but that it depends on the rate of evaporation, which is also not constant. The coefficient can range from 0.3 when the evaporation rates are high and scatters around 0.7 when the evaporation rates are lower. The researcher states that the "extra heat through the walls of the pan increases disproportionately in high-evaporation conditions". The use of a single coefficient applied year round in and of itself shows the unreliability of pan based evaporation estimates.

REMOTE SENSING

Satellite images, either Landsat or Advanced Spaceborne Thermal Emission and Reflection Radiometer (ASTER) images, hold large amounts of data that may be used to estimate evaporation. This type of data must be completely understood before it can be applied to the determination of evaporative loss from a large body of water. Data can come in different forms, calibrated and corrected or un-calibrated and un-corrected. Corrected data corrects for atmospheric conditions as well as reflection and cloud cover. Calibrated data, for example would have the temperature in a Kelvin scale rather than a

numerical scale. Also the method used to generate data from the image can give very different readings for the same scene. This is illustrated in Figure 6 below.
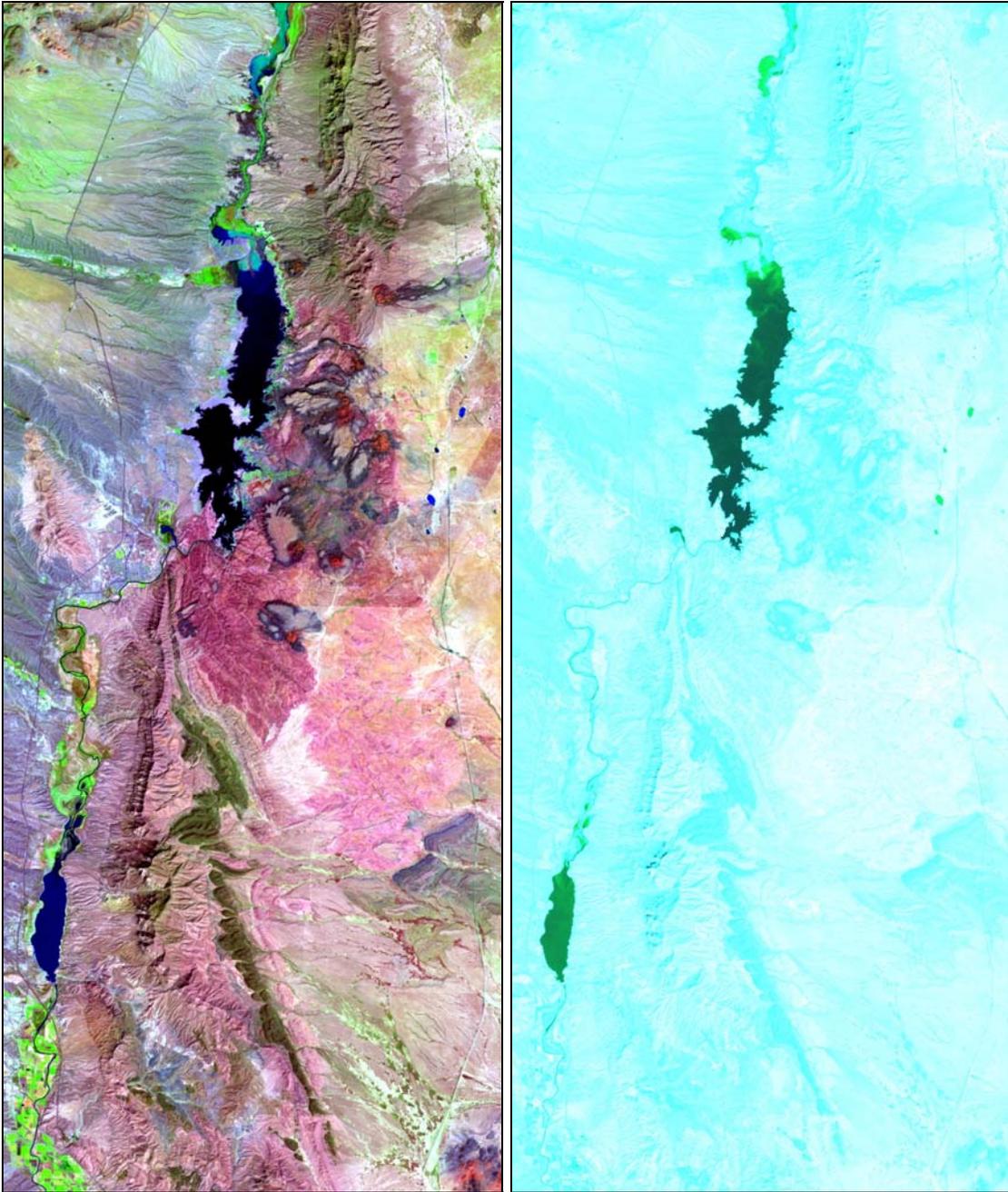

Figure 6. Satellite Images of Elephant Butte

GIS TECHNOLOGY

With the recent advances in technology, there has been a trend to integrate remote sensing with Geographical Information Systems (GIS). GIS techniques are becoming accepted in all industries and works well for analyzing and storing spatial data. A critical factor in integrating remote sensing data into a GIS is the digital nature of the data.

The major expense in dollars and man hours for a GIS is data input, since much of the data has to be converted from analog to digital form. In other words, the data has to be digitized. Satellite imagery is already in digital form and would be the foundation that other data layers could be built upon. The satellite imagery is easily transformed to fit any geographical coordinates or projections. The cost of transforming satellite imagery to a form that is acceptable to a GIS software (ArcView or ArcMap) is relatively low, and this make its use very attractive, either as a substitute for more conventional types of data, or as a completely different source of information.

The satellite imagery can be entered into the GIS in a raw form with no background or geographical reference. But the information that satellite imagery gives us is often ambiguous without other data layers or reference to location. Therefore, it is worth the extra expense and man hours to load relevant layers of data into the GIS. It is a very rare occasion that satellite imagery can yield a unique and unambiguous product without the benefit of other knowledge.

A GIS integrated with remote sensing data from satellite imagery would aid tremendously in estimating the evaporative loss from Elephant Butte Reservoir. This GIS would include information such as aerial photography of the lake, Geo-referencing data such as the USGS Index and the PLSS, the location of evaporation towers, and the locations of the weather stations. From this data the area of the lake may be determined and the remote sensing data can then be draped over all of the other data layers to complete the project and analyze the constituents of evaporative loss.

SURFACE TEMPERATURE

The surface temperature, or "skin temperature", of the reservoir is derived from the infrared bands. Figure 7 below shows a corrected image of the lake in the infrared or thermo bands. Since the image is not calibrated, the scale is numerical. From this image it appears that the lake is generally one temperature, which is much different from the surrounding land temperature (shown by the color variation). The same image has 255 colors displayed over the 1600-2300 numerical scale, with each color or number corresponding to a different temperature. In this case the lower numbers are cooler temperatures and higher numbers are higher temperatures. The same image can be tuned such that the 255 colors are only displayed over a certain region of temperatures. Figure 8 shows the same image on a numerical scale of 1600-1950. From this image the once similar lake temperatures can now be seen as very nonuniform, although uniformity is one of the major assumptions of the pan evaporation method.
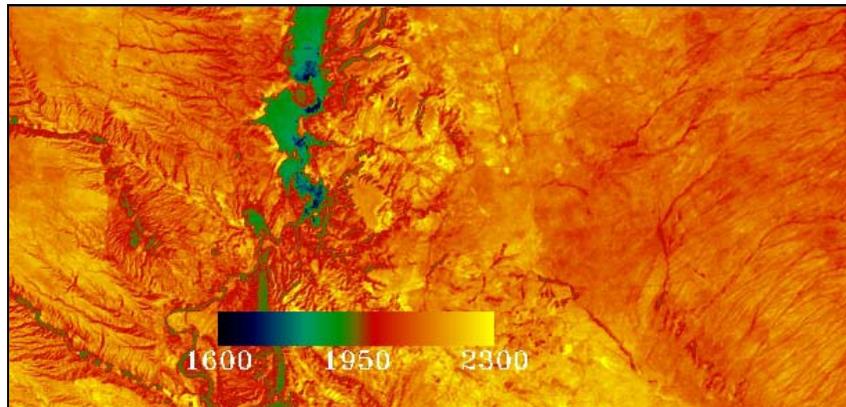
Figure 7. Elephant Butte Reservoir on June 13, 2001 (1600 to 2300 numerical scale)
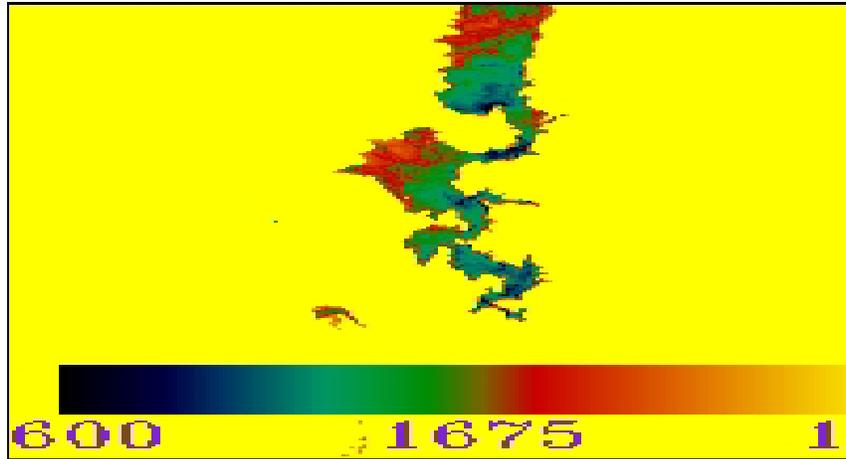
Figure 8. Elephant Butte Reservoir on June 13, 2001 (1600 to 1950 numerical scale)

A closer look at the lake is shown in Figure 9 below. The image can now be mapped and each pixel can be counted to generate the temperature gradient over the entire lake surface. The pixel size is 30 to 60 m^2 depending on whether it is Landsat or ASTER data, respectively. This information can then be used to more accurately calculate the evaporation from the lake.
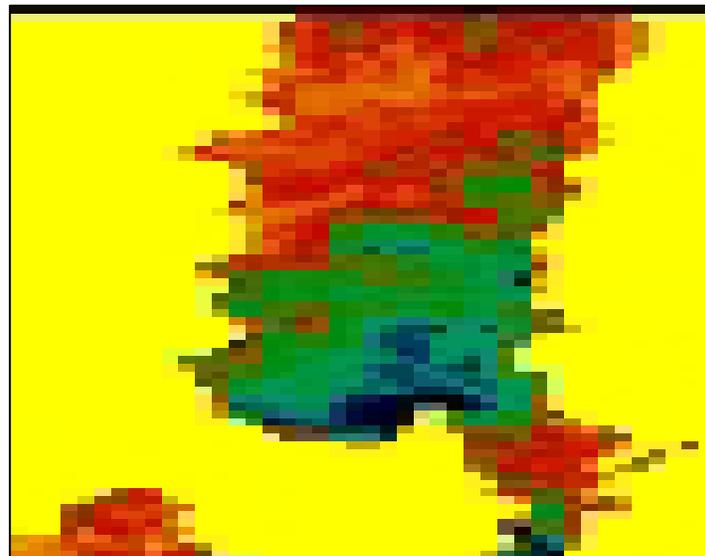
Figure 9. Elephant Butte Reservoir on June 13, 2001, Close-Up

ENVI SOFTWARE AND ASTER IMAGES

The software used to calibrate and process the remote sensing data was ENVI. ENVI is a complete remote sensing software package for analyzing and presenting digital imagery. The data came in ASTER images, which can detect thermal infrared bands that are between 0.1 μm to just over 12 μm. The ENVI software can process, calibrate, and correct the data for viewing the image, which can be manipulated in many ways. One way is to convert each pixel to a certain temperature, which would be in degrees Kelvin x 10^4. Another manipulation is to use the bandwidths for each pixel for calculations.

WIND SPEED

Wind speed is now in the developmental stages of also being able to be measured through remote sensing. Traditional methods of measuring wind speed include sensors or some windmill or turbine devices. This is effective on stable surfaces, but to use this method over the reservoir would be slightly more difficult. A raft, like the one used on Lake Tahoe as shown in Figure 10, could be configured with such an instrument, but waves and high winds could destroy the instrument.
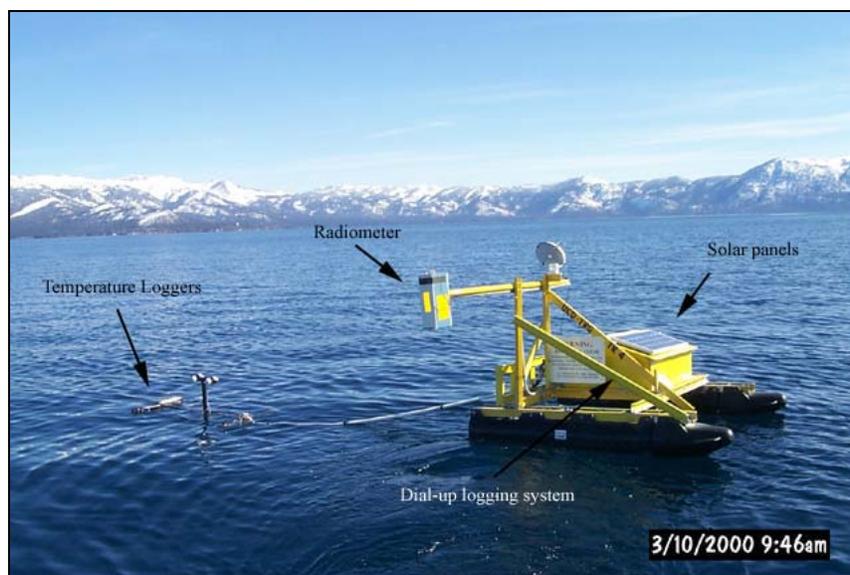
Figure 10. Raft on Lake Tahoe

Satellite images of the reservoir could prove to be a more effective method for measuring wind speed. Hasager (2003) studies the measurement of wind at distances close to the surface. The distances close to the surface are important since both the Penman equation and the Bulk-Aerodynamic method require the wind speed at 2 m above the surface. Fluxes are traditionally measured by in-situ instruments. Measurement data includes air temperature, wind speed, air humidity, and the concentration of gases at different heights above ground or water level. The report states that by using remote sensing, a roughness map of an area can be generated. The friction the wind encounters influences the wind speed near the surface. A high roughness factor of 3-4 would correspond to trees and buildings whereas a factor of 0 would be the surface of a lake. An equation of wind speed can then be applied to find the wind speed at an elevation above the surface. The graph in Figure 11 shows a typical variation of wind speed with height.
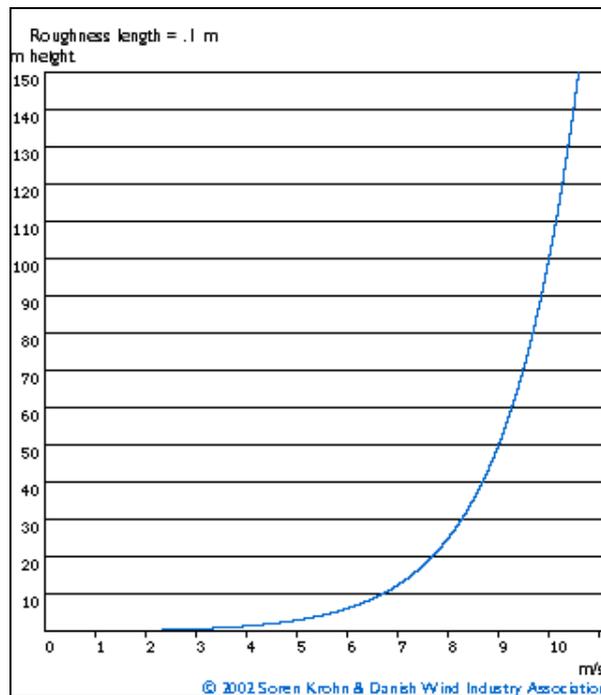
Figure 11. Variation of Wind Speed with Height

HUMIDITY GRADIENT

Humidity gradients can also be measured by remote sensing. Use of this technology is typically used for weather forecasting. Although these measurements are usually on a much larger scale the same methodology can be used to find gradients much closer to the surface of the lake. The humidity gradient can also be measured by an infrared thermocouple. An infrared sensor, type IRTS-P thermocouple (Apogee Inst. Inc.), was used at Elephant Butte Reservoir in year 2001 to measure the skin temperature of water by Bawazir and King (2003) to measure evaporation (Gamboa, 2004). The sensor accuracy and range can be seen in **Table 2**.

Table 2. Humidity Sensor Specifications

SENSOR	ACCURACY	MEASUREMENT RANGE	MAKE
Model-108 Temperature Probe	± 0.3°C	From -5° to 95°C	CSI
IRTS- P Precision Infrared Thermocouple	± 0.2°C ±0.3°C	From 15° to 35°C (± 0.2°C) From 5° to 45°C (±0.3°C)	Apogee Instruments INC
Custom Made Thermocouple (Copper and Tungsten)	± 0.3°C	N/A	N/A
HMP45 C (Temperature)	±2% over 10-90% RH ±3% over 90-100% RH	From -40° to 60°C	CSI
HMP45 C (Relative Humidity)	±0.05% RH/° C		
CR23X Data Logger	<±0.05mV		CSI
(Reference Junction Thermistor)		From -25° to 50°C	

The sensor was installed on a tower, 50 feet off-shore, which was located in 30 feet of water in 2001. The location of the tower is: 33:19.113, W107:10.384, and the elevation is 1341 m. The infrared sensor was placed 9.8 feet above the water.

PROCEDURE

Using the ASTER images with ENVI software, the different temperatures on the skin surface of Elephant Butte Reservoir was found. This can be seen in **Figure 12** below.
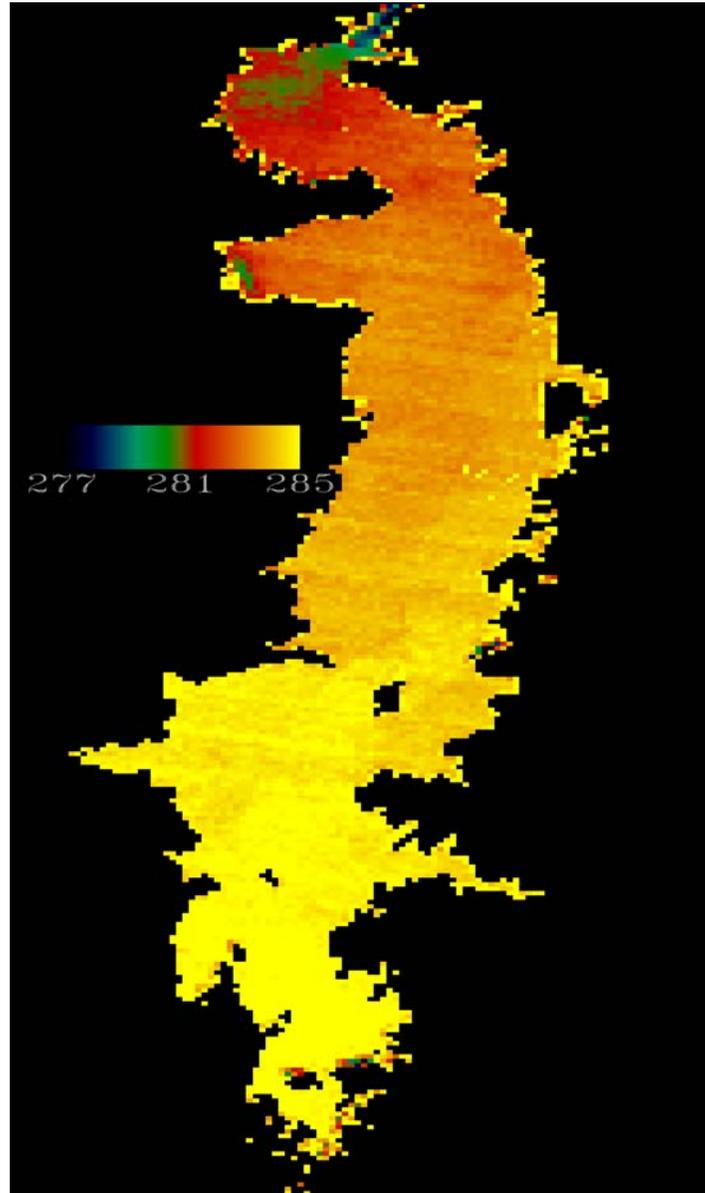
Figure 12. Elephant Butte Reservoir Temperatures in ºKelvin x 10^{4}.

In this image, darker images represent cooler temperatures while the lighter colors represent warmer temperatures. The numbers of pixels with certain temperatures were calculated and plotted using a histogram, which can be seen in **Figure 13**.
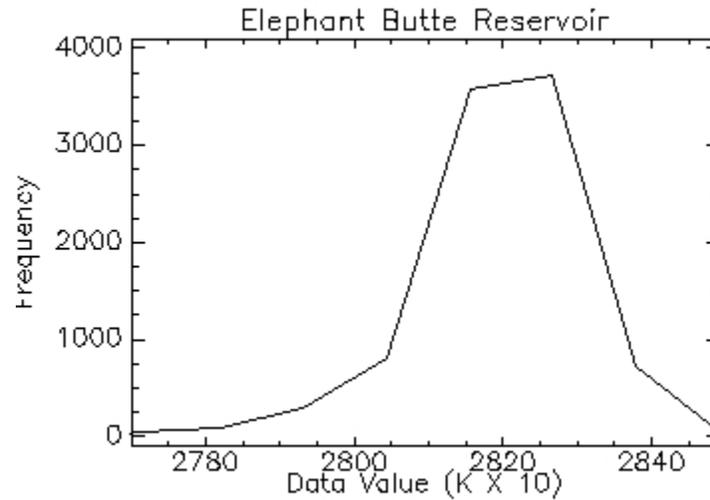
Figure 13. Histogram of Temperature Pixels

With this data, the temperatures across the entire lake can be determined. To test this method using the bulk-aerodynamic method, the tower location temperature was used from the satellite imagery, and then compared with the results from the same day for the pan data and the tower sensor. If the data was similar, then the correlation between the sensor and the satellite imagery would be confirmed. The satellite imagery could then be used and integrated across the entire lake. The data used was from December 22, 2001, in which a satellite image was downloaded, pan evaporation data was known, and bulk-aerodynamic evaporation had been calculated. The satellite image was taken at 18:00 hours GMT, so local time was 11:00 am. The location of the tower would be the comparison point to see how different the readings would be.

RESULTS ━━━━━━━━━━━━━━

As evaporation is a function of temperature, wind, and humidity, these factors are also dependent upon each other. Wind changes the humidity and if the humidity is low the evaporation rate is higher. At the same time temperature influences humidity and surface temperature. All of these factors play together to generate evaporation. Temperature may be the dominating factor that influences evaporation according to Dr. J.P. King of New Mexico State University. With this in mind, the bulk-aerodynamic method was utilized because of its reliance on the skin temperature of water and the data for December 22, 2001 was available from satellite imagery, tower sensors, and pan evaporation data. The results from this method are shown in **Table 3** below.

The temperature difference between the ASTER image and the measured temperature was 1.7º Celsius, which is significant.   When the computations were performed, the bulk-aerodynamic evaporation calculated was much higher for the ASTER image than the measured counterpart.

Table 3. Bulk-Aerodynamic Method Calculations

From Measured Data Using Bulk-Aerodynamic Method									
22-Dec	**(DOY)** Day of Year	**(T_a)** Air Temp (ºC)	**T_IRR_T_s** Skin Temp (ºC)	**(RH)** Rel. Humid (%)	**(e_a)** Vapor Pres. (kPa)	**(e_s)** Sat. Vapor Pres. (kPa)	**(U)** Wind Speed (m/s)	**(U_2)** Wind Speed at 2m (m/s)	**(E)** Evap. Rate (mm/day)
10:45	356	5.042	6.5741	49.32	0.4132	0.967	3.9607	3.179419	2.598195186
11:15	356	5.799	6.6647	41.21	0.4312	0.972	3.8907	3.123227	2.492451684
Average			6.6194				3.9257		2.545323435

From ASTER Image Using Bulk-Aerodynamic Method								
22-Dec	**DOY**	**T_a** (ºC)	**T_IRR_Ts**	**RH** (%)	**e_a** (kPa)	**e_s** (kPa)	**U_2** (m/s)	**E** (mm/day)
11:00	356	5.042	8.35	49.32	0.4132	1.224	3.151322549	3.787964081

Difference	**1.7306**							**1.242641**

Pan Evaporation Data: **E** = 0.025   mm @ 11:00 am

Bulk-Aero. Method Coef: K_E = 1.72E-08 kPa^{-1}

Note that the Bulk-Aerodynamic evaporation was calculated for just one point during the day and not for numerous points.   When tower sensor calculations are conducted, many temperatures are recorded throughout the day corresponding to the

fluctuations. This was not shown in our calculations and should be considered for future projects.

The method for estimating evaporation by Shaltout and Housry (1996) was not utilized because the data necessary to perform a linear regression was not available. However, calculations were performed using the temperatures provided, which are shown in Table 4, but the accuracy is questionable due to the fact that more data is needed. The equation for a sunny day was used, and it was found that the long-wave radiation was fairly small.

Table 4. Long Wave Radiation

Estimating evaporation by Shaltout and Housry (1996)				
Bandwidth (Kelvin $*10^4$)	SQRT (e_s)	R (long wave radiation)		
2781.964706	1.1065367	4285.524	0.428552	mJ/m^2
2793.137255	1.1065367	4302.841	0.430284	mJ/ m^3
2804.309804	1.1065367	4320.159	0.432016	mJ/ m^4
2815.482353	1.1065367	4337.476	0.433748	mJ/ m^5
2826.654902	1.1065367	4354.794	0.435479	mJ/ m^6
2837.827451	1.1065367	4372.111	0.437211	mJ/ m^7
2849.000000	1.1065367	4389.429	0.438943	mJ/ m^8

CONCLUSIONS

There are many assumptions that go into these calculations. The wind temperature used is assumed to be constant throughout the lake, which it is not. Also, the exact time for both the satellite image and the measured data has to be identical in order to compare the evaporation values. Also, the measured bulk-aerodynamic method had many measured points at different times of the day, where the ASTER image was at only one time. If we could obtain many ASTER images from one day, then a more accurate calculation would be acquired. We didn't have all of the necessary data values for calculating the evaporation loss using the Penman equation, so more research needs to be performed.

However, overall, a conclusion can be made that pan evaporation is not the most accurate and precise method of evaporation measurement, and that the use of remote sensing shows promising results. Further research and comparison of results need to be

explored for a better understanding of the primary constituents of evaporation and its measurement.   Although evaporation is not necessarily preventable, evaporation predictions can be improved. The implications of better predictions are far reaching, not only to the Elephant Butte Reservoir and the lower Rio Grande River, but to other bodies of water as well. Examples of using better predictions would be better preparation of water allotments and allocation. Other implications of more accurate knowledge of evaporation could even change court cases that battle over water-use and allotment. An example of such is William Turners written testimony in the hearing of the Silvery Minnow Impact on New Mexico, at which he refers numerous times to evaporation and how it is a loss of water greater than the total usage of municipal use and the Silvery Minnow combined. The numbers he uses are, of course, from pan evaporation data. And actually the water lost to evaporation is not lost, but goes into the water cycle. Clearer understanding of evaporation and more accurate measurement thereof will be beneficial to all, especially those states like New Mexico, that are located in arid regions of the United States.

The bulk-aerodynamic method is very promising, and seems to also be the best fit for estimating evaporation using satellite imagery. Further research and data collection is recommended to continue with the progress that has been made.

APPENDIX - EVAPORATION EQUATIONS

Penman's Equation

Penman's equation (Penman, 1948, 1963; Shuttleworth, 1993) estimates evaporation from the free surface of a body of water (potential evaporation) by considering what is necessary to balance the energy budget at the water surface. The potential evaporation [mm d^{-1}] is a fairly complex function of humidity, wind speed, radiation, and temperature:

$$E_P = \frac{\Delta}{\Delta + \gamma}\left(R_n + A_h\right) + \frac{\gamma}{\Delta + \gamma}\frac{6.43\left(1 + 0.536U_2\right)D}{\lambda}$$

where

R_n = net radiation exchange (water equivalent) at the surface of the body of water [mm d^{-1}],

A_h = energy advected to the water body (water equivalent) [mm d^{-1}],

(Shuttleworth, 1993) provides an elaborate procedure to estimate (R_n+A_h) from alternative sources of data.)

D = average vapor pressure deficit (e_s-e) over the estimation period [kPa]. This can be estimated as (Shuttleworth, 1993):

$$D = \left(\frac{e_s\left(T_{max}\right) + e_s\left(T_{min}\right)}{2}\right)\left(1 - \frac{RH}{100}\right)$$

T_{max}, T_{min} = max and min temperatures over the period of estimation [°C],

RH = average relative humidity over the period of estimation [percent],

U_2 = wind speed measured at 2m elevation [m s^{-1}],

λ, a function of temperature, is the latent heat of vaporization of water at temperature T (the surface temperature of the water body, °C) [MJ kg^{-1}]:

$$\lambda(T) = 2.501 - 0.002361T_s$$

e = the ambient vapor pressure of water vapor in the air [kPa], which can be calculated from the relative humidity and the saturated vapor pressure:

$$e = e_s\frac{RH}{100}$$

RH = relative humidity of the air [percent],

e_s, a function of temperature, is the saturated vapor pressure of water in air at temperature T [kPa]:

$$e_s(T) = 0.6108 \exp\left(\frac{17.27T}{237.3 + T}\right)$$

Δ, the rate of change of e_s with respect to T [kPa T^{-1}]:

$$\Delta(T) = \frac{4098 e_s}{(237.3 + T)^2} = \frac{2503.06 \exp\left(\dfrac{17.27T}{237.3 + T}\right)}{(237.3 + T)^2}$$

γ = the 'psychrometric constant' [kPa °C^{-1}]:

$$\gamma = 0.0016286 \frac{P}{\lambda} = \frac{P}{1537.675 - 145T}$$

At sea level elevation, P = 101.3 [kPa].

Hargreaves' Equation

Hargreaves equation (Hargreaves, 1975) is recommended by Shuttleworth (1993) as one of the few valid temperature-based estimates of potential evaporation, though it was designed for estimating potential evaporation for agricultural systems. It gives an estimate of potential evaporation (mm d^{-1}), which can be averaged to obtain monthly values:

$$E = 0.0023 S_o (T + 17.8) \sqrt{\delta_T}$$

where

T = temperature [°C],

δ_T = difference between mean monthly maximum temperature and mean monthly minimum temperature [°C], (i.e. the difference between the maximum and minimum temperature for the given month, averaged over several years),

S_o = the water equivalent of extraterrestrial radiation [mm d^{-1}] for the location:

$$S_o = 15.392 d_r (\omega_s \sin \phi \sin \delta + \cos \phi \cos \delta \sin \omega_s)$$

ϕ = latitude of the site (+ in northern hemisphere, - in southern),

ω_s = the sunset hour angle [radians]:

$$\omega_s = \arccos(-\tan \phi \tan \delta)$$

δ = solar declination on day J (Julian day) of the year [radians]:

$$\delta = 0.4093 \sin\left(\frac{2\pi}{365} J - 1405\right)$$

d_r = relative distance of the earth from the sun on day J:

$$d_r = 1 + 0.033 \cos\left(\frac{2\pi}{365} J\right)$$

Hamon's Equation

One of the simplest estimates of potential evaporation is that of Hamon (1961), used to estimate seasonal (monthly) or annual values. Following Haith and Shoemaker (1987), Hamon's estimate of potential evaporation is:

$$E = \frac{2.1 H_t^2 e_s}{\left(T_t + 273.2\right)}$$

where

E = evaporation, day t [mm day^{-1}],

H_t = average number of daylight hours per day during the month in which day t falls,

e_s = saturated vapor pressure at temperature T [kPa] (see Penman's equation above),

T_t = temperature, day t [°C],

H_t can be calculated by using the maximum number of daylight hours on day t, N_t. that is

$$N_t = \frac{24\omega_s}{\pi}$$

where ω_s is the sunset hour angle of day t (see Hargreave's equation above). On days when

T_t <= 0, Haith and Shoemaker set E = 0. Daily values of E are then summed over the period

of interest to obtain the monthly or annual estimate.

Wind Equation

Wind Shear Formula:

The wind speed at a certain height above ground level is:

$$v = v_{ref} \frac{\ln\left(\dfrac{z}{z_o}\right)}{\ln\left(\dfrac{z_{ref}}{z_o}\right)}$$

where

v = wind speed at height *z* above ground level,

v ref = reference speed, i.e. a wind speed we already know at height z_{ref}. (Note: ln(...) is the natural logarithm function).

z = height above ground level for the desired velocity, *v*.

z 0 = roughness length in the current wind direction.

Roughness lengths may be found in the *Wind Energy Reference Manual (2003)*.

z ref = reference height, i.e. the height where we know the exact wind speed v_{ref}.

Bulk-Aerodynamic Method

The bulk-aerodynamic equation is used to estimate evaporation. The coefficient, K_E, reflects the efficiency of vertical transport of water vapor by turbulent eddies of the wind.

$$E = K_E u (e_s - e_a)(86.4x10^6)$$

where

E = evaporation rate [mm day^{-1}],

K_E = coefficient [kPa^{-1}],

u = wind speed measured at 2 m above the surface as standard [m s^{-1}],

e_s = saturation vapor pressure at the water surface [kPa],

e_a = vapor pressure of the air above the water surface [kPa],

86.4 x 10^6 = conversion factor.

K_E is determined as follows:

$$K_E = \frac{0.622\rho_a}{P\rho_w} \frac{0.4^2}{\left[\ln\left(\frac{z_m - z_d}{z_o}\right)\right]^2}$$

where

K_E = coefficient of efficiency of vertical transport of water vapor by eddies of the wind [kPA^{-1}],

ρ_a = density of air [1.220 kg m^{-3}],

ρ_w = density of water [1000 kg m^{-3}],

P = atmospheric pressure [kPa],

Z_m = height at which wind speed and air vapor pressure are measured [m],

Z_d = zero-plance displacement [m]; Z_d = 0 over typical water surfaces[*],

Z_o = roughness height of the surface [m]; Zo = 2.30 x 10^{-4} m over typical water surfaces[*],

Atmospheric pressure at the site was determined by the following equation from Jensen and others (1990).

---

[*] Values obtained from Brutsaert (1982) as suggested by Dingman (2002). The Z_o and Z_d increase as wind speed increases due to the effects of waves.

$$P = 101.3 \left[\frac{288 - 0.0065E}{288} \right]^{5.257}$$

where

P = atmospheric pressure [kPa],

E = elevation above sea level [m],

Wind speed was measured at about 20 ft (6 m) above the water surface. But in order to compare with other methods such as Penman combination, the wind speed was adjusted to 6.6 ft (2 m) height "standard." The depth of water was declining during the measurement period. However, the wind speed sensor remained at a height range between 6 to 10 m. Wind speed was adjusted to 2 m height by using equation 4 following Jensen and others (1990).

$$U_2 = U_6 \left(\frac{z_2}{z_6} \right)^{0.2}$$

where

U_2 = wind speed measured at 2 m [m s^{-1}],

U_6 = wind speed measured at 6 m [m s^{-1}],

z_2 = height of 2 m,

z_6 = height of 6 m.

Saturation vapor pressure, e_s, of the air is a property that is dependent on temperature and was estimated by polynomial function (Lowe 1977). Water surface temperature or "skin" temperature was used to determine the saturation vapor pressure at the water surface. Vapor pressure of the air was determined by multiplying relative humidity with saturated vapor pressure. In this case, saturated vapor pressure of air was determined by using the air temperature.

$$e_s = \frac{a_0 + T(a_1 + T(a_2 + T(a_3 + T(a_4 + T(a_5 + a_6 T)))))}{10}$$

where

e_s = saturation vapor pressure [kPa],

T = temperature [°C],

a_o = 6.1078,
a_1 = 4.4365 x 10^{-1},
a_2 = 1.42895 x 10^{-2},
a_3 = 2.65065 x 10^{-4},
a_4 = 3.30312 x 10^{-6},
a_5 = 2.03408 x 10^{-8},
a_6 = 6.13683 x 10^{-11}.

REFERENCES ━━━━━━━━━━━━━━━━━━

Bawazir, A. S. and King, J. P. (2003). Evaporation Estimation at Elephant Butte Reservoir, Las Cruces, NM.

Brutsaert, W. (1982). *Evaporation into the Atmosphere: Theory, History, and applications.* D. Reidel Publ. Co., Dordrecht, Netherlands. 299 p.

Dingman, S. L. (2002). *Physical Hydrology*. – 2nd edition. Prentice-Hall, Upper Saddle River, New Jersey. x,646 p.

Gamboa, M. (2004). Using Bulk-Aerodynamic Method and Skin Temperature of Water to Estimate Evaporation of Elephant Butte Reservoir, Las Cruces, NM.

Haith, D. A. and Shoemaker, L. L. (1987). Generalized Watershed Loading Functions for Stream Flow Nutrients. *Water Resources Bulletin* 23:471-478.

Hamon, W.R. (1961). Estimating Potential Evapotranspiration, *Journal of the Hydraulics Division, ASCE.* 87(HY3):107-120.

Hargreaves, G.H. (1975). Moisture Availability and Crop Production, *Trans. Am. Soc. Agric. Eng.* 18(5):980-984.

Jensen, M. D., R. D. Burman, and R. G. Allen, Eds. (1990). *Evapotranspiration and Irrigation Water Requirements.* ASCE Manuals and Reports on Engineering Practice no.70. American Society of Civil Engineers, New York. 332 p.

Linacre, E. (1994). Estimating Us Class A pan evaporation from few climate data. Water International, 19: 5-14.

Lowe, P.R. (1977). "An approximating polynomial for the computation of saturation vapor pressure." *Journal of Applied Meteorology.* 16:1:100-103.

Mosner, M.S. and Aulenbach, B.T. (2003). Comparison of Methods Used to Estimate Lake Evaporation for a Water Budget of Lake Seminole, Southwestern Georgia, and Northwestern Florida. Proceedings of the 2003 Georgia ater Resources Conference, April 23-24, Athens, Georgia.

Penman, H.L. (1948). Natural Evaporation from Open Water, Bare Soil, and Grass. *Proc. R. Soc.*, London, Vol A193:120-145.

Penman, H.L. (1963). Vegetation and Hydrology, *Tech. Comm. 53.* Commonwealth Bureau of Soils, Harpenden, England.

Priestly, C.H.B. (1982). Reminiscenes of 30 years of meteorological research in australia, Australian Meteorological Magazine, Vol. 30, 19-30.

Sabins, F. F. (1997). Remote Sensing: Principles and Interpretation, W.H. Freeman and Company, 3rd Edition, New York, 432 pp.

Shaltout, M. A. M. and Housry , T. (1996). Estimating the Evaporation over Nasser Lake in the Upper Egypt From Meteosat Observations, *S096.1.016*, Cairo, Egypt.

Shuttleworth, W.J. (1993). Evaporation, Ch.4, <u>In</u> D.R. Maidment (ed.), *Handbook of Hydrology*, Mcgraw-Hill, various pagings.

INTERNET REFERENCES

ASTER, Advanced Spaceborne Thermal Emission and Reflection Radiometer.
http://asterweb.jpl.nasa.gov/

EBID, Elephant Butte Irrigation District. About EBID. 2003.
http://www.ebid-nm.org

ENVI, Environment for Visualizing Images
http://www.rsinc.com/envi/index.asp

Hasager, C. (2003). Aggregation of Surface Fluxes. Risoe National Laboratory.
http://www.risoe.dk/

Hearing on the Silvery Minnow Impact on New Mexico. Written testimony of W. Turner. Sept 2003. US House of Representatives, Washington D.C.
www.waterbank.com/Newsletters/nws44.html

Wind Energy Reference Manual Part 1: Wind Energy Concepts. Danish Wind Industry Association (2003).
http://www.windpower.org/en/stat/unitsw.htm#roughness

Wind Speed Measurement in Practice. Danish Wind Industry Association (2002).
http://www.windpower.org/en/tour/wres/wndsprac.htm